Anomalous Pressure Dependence of the Electronic Properties of Molecular Crystals Explained by Changes in Intermolecular Electronic Coupling

Maituo Yu¹, Xiaopeng Wang¹, Xiong-Fei Du¹, Christian Kunkel², Taylor Garcia³, Stephen Monaco³, Bohdan Schatschneider³, Harald Oberhofer², and Noa Marom^{1,4,5}

Abstract: Optimization of the electronic properties of crystalline organic semiconductors is important for the evolution of organic optoelectronic devices. One method of tuning the electronic properties is by applying external pressure to semiconducting molecular crystals. A recent dispersion-inclusive density functional theory (DFT) investigation regarding the effect of pressure up to 20 GPa on herringbone polycyclic aromatic hydrocarbons (PAHs) has revealed anomalous pressure dependence of the electronic properties of six systems [J. Phys. Chem. C 122, 23828 (2018)]. Here, we use intermolecular electronic coupling values (H_{ab}), calculated by fragment orbital DFT (FO-DFT) to elucidate the pressure dependence of the electronic properties. We show that discontinuities in the pressure dependence of the band structures are correlated with pressure-dependent discontinuities in the electronic couplings of certain molecular dimers. H_{ab} is shown to be a useful descriptor for gaining insight into the pressure dependence of the electronic properties of crystalline organic semiconductors.

1. Introduction

Organic semiconductors have attracted substantial attention for applications in electronic and optoelectronic devices such as organic photovoltaics (OPV), organic light-emitting diodes (OLEDs), and field-effect transistors.^{1–3} Efficient operation of various electronic devices poses different requirements on the optimal electronic properties of a semiconductor. Semiconductors for OPV require smaller band gaps to increase the wavelength of sunlight that can be absorbed by the device. In turn, this increases the number of electrons excited from the highest occupied molecular orbital (HOMO), thereby increasing the theoretical efficiency of the solar cell.⁴ For OLEDs, the color emitted by the device is determined by the band gaps of the semiconductors. Recombination of electrons and holes at specific energy levels causes the emission of photons with different colors. Advantageously, the vast chemical compound space of organic semiconductors enables tuning their electronic and optical properties by chemical substitution with functional

¹Department of Materials Science and Engineering, Carnegie Mellon University, Pittsburgh, PA 15213, USA

²Chair for Theoretical Chemistry and Catalysis Research Center, Technische Universiät München, Lichtenbergstr. 4, D-85747 Garching, Germany

³Department of Chemistry and Biochemistry, California State Polytechnic University at Pomona, Pomona, CA 91768, USA

⁴Department of Physics, Carnegie Mellon University, Pittsburgh, PA 15213, USA

⁵Department of Chemistry, Carnegie Mellon University, Pittsburgh, PA 15213, USA

groups, which may affect the single molecule properties, as well as the crystal structure and the solid state properties. 5-8

Molecular crystals of organic semiconductors may exhibit polymorphism, where the same molecule forms different crystal structures. Polymorphic crystals may display diverse optoelectronic properties, including charge-carrier mobility, which ultimately influences organic electronic device operation. 9–11 The key to charge transport in organic materials is the ability of charge-carriers to move from one molecule to another either through a hopping mechanism or *via* band transport. Regardless of the transport mode, the carrier mobility has a strong dependence on the molecular packing within the crystal. 6,12 The nature and strength of intermolecular interactions between adjacent molecules affects the electronic coupling between their frontier orbitals and thereby the carrier mobility. Hence, one way to tune the carrier mobility may be *via* modification of the intermolecular interactions within the crystal structure.

External pressure may be used to tune the intermolecular interactions of organic semiconductor crystals. In some cases it induces polymorphic phase transitions. These structural rearrangements ultimately lead to changes in the optoelectronic properties. A recent example of this lies in the experimentally measured pressure-dependent red-shift of the optical gap in paradiiodobenzene. A second example is the computationally predicted pressure dependent narrowing of the optical gap for a series of herringbone polycyclic aromatic hydrocarbons (PAHs). A third example lies in the pressure dependent increase of the carrier mobility and photoconductivity of phenanthrene, chrysene, picene, tetracene and pentacene. Control over these pressure-induced modifications could be beneficial to the performance of organic semiconductors in device applications.

Among organic semiconductors, PAHs have been widely studied because of their unique optoelectronic properties such as their relatively small band gaps and high mobility values. PAHs in this context are composed entirely of aromatic-carbon and hydrogen atoms. The coupling of the extended π -orbitals in PAHs may produce efficient charge transfer and relatively large mobility values. PAHs may produce efficient charge transfer and relatively large mobility values. PAH molecular crystals typically increases the electronic coupling between adjacent molecules by increasing the C···C (π ··· π) and C···H intermolecular close contacts while decreasing the H···H contacts. Phenomenation in the pressure induced decrease in intermolecular distances may also cause molecular deformation. The combination of these structural changes may lead to significant alteration of the optoelectronic properties, including the band structure and carrier mobility. PAHs and high mobility values. PAHs in the contact of the properties of the properties of the properties of the properties of the properties.

Here, we investigate six HB PAH crystals, whose electronic properties were previously found to exhibit anomalous pressure dependence, which manifests as discontinuous changes in the band structure with increasing pressure. 13 In many cases, changes in the electronic properties are correlated with changes in structural descriptors such as the lattice parameters and the Hirshfeld intermolecular close contact fractions.^{25,26} Moreover, significant conformational changes are observed in some molecules, which may further modify the electronic properties by changing the molecular orbital energies. For three of the materials studied here, [14]annulene (FANNUL), benzo[b]triphenylene (SANQII), and 1,8-dipyrenylnaphthalene (CENYAV), pressure-induced changes in the band structure correspond to discontinuities in the pressure dependence of the lattice fractions. Hirshfeld close contact 9-(4-7,14biphenyl)cyclopenta[a]phenalene (ABECAL), [5]helicene (DBPHEN02), diphenyldibenzo (KAGFOP) exhibit discontinuous changes in the band structure under pressure, while their lattice parameters display a nearly continuous pressure dependence. 13,15

To explain the anomalous pressure response of these materials, we use intermolecular electronic coupling values, denoted as H_{ab} . These are calculated *via* fragment orbital DFT (FODFT)^{27–30}, whereby the charge localized diabatic states are constructed from non-interacting fragment densities. Here, the fragments are the isolated donor and acceptor molecules involved in the charge transfer process. H_{ab} , also known as the diabatic coupling or transfer integral,²⁷ is the off-diagonal matrix element of the initial state, Ψ_a , and final state Ψ_b :

$$H_{ab} = \langle \Psi_a | \widehat{\mathcal{H}} | \Psi_b \rangle \tag{1}$$

where $\widehat{\mathcal{H}}$ is the Hamiltonian of the system. The calculation of H_{ab} is the most critical step in the determination of polaronic hopping rates, which are important for calculating carrier mobility. Moreover, based on the Marcus theory, the charge transfer rate is directly related to the square of the absolute value of H_{ab} . H_{ab} also reflects the quantum mechanical overlap of the frontier orbitals involved in the charge transport and therefore may influence other electronic properties, such as the band structure.

In the following, we show that discontinuous changes in the band structures of some HB PAHs under pressure can be explained by corresponding discontinuous changes in the H_{ab} values of certain molecular dimers in their crystal structures. Subtle changes in the internal structure of the unit cell may lead to significant and discontinuous changes in the intermolecular electronic coupling even when the lattice parameters appear to vary smoothly. Thus, H_{ab} is a useful tool for elucidating the anomalous pressure dependence of the electronic properties of the HB PAHs studied here.

2. Methodology

The geometry of the HB PAHs studied here was obtained from Ref. 15. Therein, geometry optimization was performed under isotropic pressures between 0 and 20 GPa in 0.5 GPa increments, starting with structures found in the Cambridge Structural Database (CSD)^{34–39}. This was performed with the CASTEP density functional theory (DFT) code⁴⁰ using the Perdew-Burke-Ernzerhof (PBE)⁴¹ generalized gradient approximation coupled to the pairwise dispersion method of Tkatchenko-Scheffler (TS).⁴² Norm-conserving pseudopotentials were utilized for C and H atoms. The plane-wave basis set cut-off was 750 eV and the k-point grid spacing was 0.07 Å⁻¹. The convergence criteria for total energy, maximum force, maximum stress, and maximum displacement were 5×10^{-6} eV per atom, 0.01 eV Å⁻¹, 0.02 GPa, and 5×10^{-4} Å, respectively. ^{13,15} All geometry optimized structures (at each pressure) can be found in the Organic Molecular Crystal Properties Database (OMCPD) at www.organiccrystalbandgaps.org

Band structure calculations were performed for each crystal at all pressures, using the PBE functional with the tight/tier2 basis sets of the FHI-aims package. The PBE calculations were performed with k-grids of $4 \times 4 \times 4$ for ABECAL and KAGFOP, $4 \times 8 \times 4$ for FANNUL and SANQII, and $8 \times 4 \times 4$ for CENYAV and DBPHEN02. The path in reciprocal space used for the six PAHs studied here is along the high symmetry k-points of Γ (0, 0, 0), Γ (0, 0, 0), Γ (0, 0, 0), Γ (0, 0, 0), Γ (1), Γ (1), Γ (2), Γ (3), Γ (3), Γ (4), Γ (5), Γ (6), Γ (7), Γ (8), Γ (8), Γ (9), Γ (9)

The band dispersion is defined here as the energy difference between the high and low energy values of the highest energy HOMO-derived or the lowest energy LUMO-derived bands. According to this definition, most of the materials studied here are *n*-type semiconductors under

ambient pressure, where the LUMO derived conduction band is more dispersed than the HOMO-derived valence band, except for CENYAV, which is *p*-type. DBPHEN02, ABECAL and SANQII switch polarity under pressure, as discussed below. We note that a different definition of the band dispersion was used in Ref. ¹³. Therein, the band dispersion was defined as the energy difference between the high energy limit and low energy limit of the top valence band and the bottom conduction band.

Electronic coupling values (H_{ab}) were calculated for each crystal at all pressures, using the fragment molecular orbital approach (FO-DFT), 45,46 implemented in the FHI-aims package. This calculation is performed in two steps. The first is to calculate the individual molecular orbitals of two neighboring molecules in the unit cell and the second is the construction of the Hamiltonian from the superposition of the two fragment densities. To construct a Hamiltonian that corresponds to hole transfer from a singly positively charged donor fragment, D^+ , and a neutral acceptor fragment, A, the $\mathcal{H}^{2n-1}@D^+A$ variant of FO-DFT was employed here, where 2n-1 is the number of electrons used to construct the Hamiltonian. Conversely, to construct a Hamiltonian that corresponds to electron transfer, the $\mathcal{H}^{2n+1}@D^-A$ variant of FO-DFT was employed, where D^- is a singly negatively charged donor fragment, A is a neutral acceptor fragment, and 2n+1 is the number of electrons used to construct the Hamiltonian.

H_{ab} values were calculated for all the unique dimers between neighboring molecules in each PAH crystal. For each crystal, a 2 × 2 × 2 supercell was generated. Every pair of molecules in the supercell was considered as a dimer. The dimer geometries were extracted from the aforementioned crystal structures under pressure up to 20 GPa without any further optimization. Dimers were discarded if they were duplicates or if the distance between the center of mass of two molecules was too large to observe a H_{ab} value. A threshold distance of 5 Å was used here. The Becke exchange functional in combination with the correlation functional of Lee, Yang, and Parr (BLYP)^{47,48} was employed because it has been proven to provide the best accuracy in the calculation of hole transfer H_{ab}.²⁷ FHI-aims calculations were performed with tier-2 numeric atomic orbital basis sets and tight integration grids. For each material, only the dimers that exhibit the most significant discontinuities in their H_{ab} values under pressure are shown in the main text. Representative results for additional dimers are provided in the SI. Both hole transfer and electron transfer Hab values are provided for comparison. In general, the Hab values for hole transfer and electron transfer are found to display discontinuities at the same pressures. We note that the focus of the present study is on structural properties at 0K, disregarding the effect of e.g., electronphonon couplings, which can also be strongly influenced by pressure-dependent structural changes.

To visualize the fragment density overlap around the discontinuities in H_{ab} , the HOMO of each fragment was calculated employing the same method used for the H_{ab} calculations. The HOMO charge density was then written to a uniform three-dimensional grid of $100 \times 100 \times 100$ voxels, using the ASCII-based cube file format. The orbital overlap was obtained from the two cube files by multiplying the density values at each voxel. For each system, the orbital overlaps were visualized under different pressures using the same isosurface value.

The internal geometries and intermolecular interactions of all crystals were also studied as a function of pressure using Hirshfeld surface analysis. Hirshfeld surfaces are generated from the 0.5 isosurface of the weight function constructed using Bondi van der Waals radii. 49,50 Once the isosurface is calculated, it can be partitioned according to the atoms used in its construction (*i.e.*, the internal and external nuclei contacting the surface). Therefore, interactions between atoms from different molecules can be monitored as a function of partitioned atom-atom close contacts at the surface. Production of fingerprint plots from the partitioned Hirshfeld surface can provide

the relative fractions of atom-atom intermolecular close contacts at the surface between interacting fragments. This, in turn, allows one to analyze the crystalline internal geometry as a function of pressure via the intermolecular close contact fractions. Explanations of Hirshfeld surfaces and their applications are provided in Refs ^{49–51}. An important difference between Hirshfeld surface analysis and H_{ab}, is that the former is calculated based on the total charge density of the molecules, whereas the latter is calculated based on the specific molecular orbitals involved in charge transport.

3. Results and discussion

3.1. Band structure changes accompanied by significant discontinuities in the lattice parameters

3.1.1. [14] Annulene (FANNUL)

FANNUL is an aromatic hydrocarbon monocycle with 14π electrons.⁵² It crystallizes in a monoclinic polymorph with a P2₁/c space group and two molecules in the unit cell, as shown in Fig. 1(a). Due to the presence of four hydrogen atoms at the molecule's center, the molecule shows

significant nonplanarity.³⁹ Two dimers, labeled "dimer **a**" and "dimer **b**" are displayed in Fig. 1(a). Dimer **a** consists of two neighboring molecules along the a direction, whereas dimer **b** consists of two neighboring molecules along the b direction.

The lattice parameters of FANNUL as a function of pressure are plotted in Fig. 1(b). Pressure-dependent discontinuous changes are observed between 1.5 and 2.0 GPa, as well as between 4.0 and 4.5 GPa. At the first discontinuity, the *a* and *c* parameters shrink by 3.0% and 6.0%, respectively, while the *b* parameter increases by 5.9%. At the second discontinuity, the changes are 2.9%, 4.4% and 4.1% for *a, b,* and *c,* respectively. There are several minor discontinuities above 4.5 GPa. These discontinuities also manifest in the Hirshfeld surface analysis, provided in the SI.

The discontinuities in the structural parameters correspond to discontinuous changes in the band structure, as shown in Fig. Additional plots of the pressure dependence of the band gap and band dispersion are provided in the SI. The shape of the bands remains almost the same throughout the entire pressure range. The valence band maximum (VBM) and the conduction band minimum (CBM) always appear at the high symmetry points Γ (0, 0, 0) and B (-0.5, 0, 0), respectively, indicating an indirect band gap. The largest

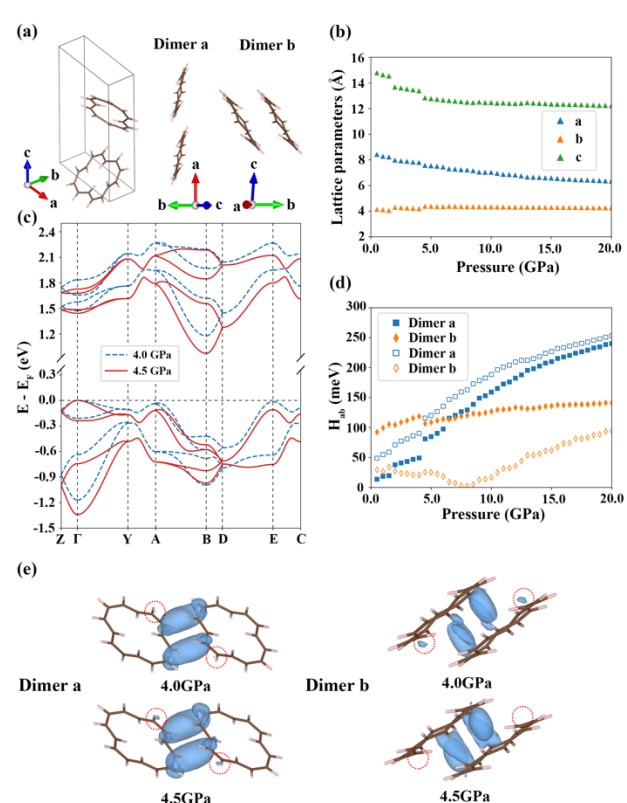


Fig. 1. (a) The FANNUL unit cell. Dimer **a** is stacked along the *b* direction and dimer **b** is stacked along the *a* direction. (b) Pressure dependence of the lattice parameters. (c) Band structures of FANNUL at 4.0 GPa and 4.5 GPa with the valence band maximum (VBM) referenced to 0 eV. (d) Pressure dependence of the H_{ab} of dimer **a** and dimer **b**, the full marker represents the electron transfer H_{ab} and empty marker represents the hole transfer H_{ab} . (e) Overlap of the HOMOs of the molecules comprising dimer **a** at the pressures near the discontinuity.

discontinuities in the band structure exist between 4.0 and 4.5 GPa. The HOMO derived band dispersion increases by 0.156 eV and the LUMO derived band dispersion increases by 0.113 eV as a result of increasing pressure, resulting in a narrowing of the band gap by 0.205 eV.

The pressure-dependent discontinuities in the structural descriptors and electronic properties are consistent with discontinuities in the pressure-dependent Hab values of dimer a and dimer **b**, as shown in Fig. 1(d). The hole transfer H_{ab} value of dimer **a** increases by 12.19 meV from 1.5 to 2.0 GPa, and by 25.49 meV from 4.0 to 4.5 GPa. The electron transfer H_{ab} increases by 18.12 and 31.87 meV, respectively, at the same pressures. The larger increase in the electron transfer H_{ab} compared to hole transfer H_{ab} between 4.0 to 4.5 GPa is consistent with the larger increase in the conduction band dispersion compared to the valence band dispersion. Compared to dimer a, the electron and hole transfer H_{ab} of dimer b shows smaller discontinuities. However, the electron transfer Hab values of dimer **b** are always larger than the hole transfer Hab values. This result is consistent with the n-type polarity of FANNUL, as evident from the band dispersion shown in the SI. The discontinuity in the H_{ab} values between 4.0 to 4.5 GPa for dimer a can be related to the overlap of HOMOs of the two molecules, as shown in Fig. 1(e). The overlap at 4.5 GPa is noticeably greater than at 4.0 GPa, in particular in the areas circled in red (a magnified view is provided in the SI). In summary, for FANNUL, the pressure-dependent discontinuities of the structural descriptors and Hab are correlated with the discontinuous changes in the band structure occurring around 2.0 and 4.5 GPa.

3.1.2. Benzo[b]triphenylene (SANQII)

The monoclinic polymorph of SANQII, shown in Fig. 2(a), has a P2₁ space group. There are four molecules per unit cell, with two symmetry inequivalent molecules, α and β , displayed in red and blue, respectively. The molecular π -stacking in the crystal is along the b axis for both the α and β molecules.³⁷ Two dimers, labeled **a** and **b**, are shown in Fig. 2(a). Dimer **a** consists of two adjacent α molecules along the b axis. Dimer **b** consists of two adjacent β molecules in the same direction. Fig. 2(b) shows the pressure dependence of the lattice parameters of SANQII. As the pressure increases, the lattice parameters decrease continuously up to 7.5 GPa, where a discontinuity is observed. The a and c parameters increase by 9.9% and 8.4%, respectively, from 7.5 to 8.0 GPa. Conversely, the b parameter, which corresponds to the π -stacking direction, decreases by 16.4%. The elongation of a and c combined with the shrinkage of b, cause the angle between the molecular plane and the ac plane to decrease. These discontinuities also manifest in the Hirshfeld surface analysis, provided in the SI.

Because the π -stacking of SANQII is along the b direction, which corresponds to the b_2 reciprocal vector, there should be strong electronic couplings between molecules stacked along b in real space and larger band dispersion along paths with a significant b_2 component in reciprocal space. Indeed, as shown in Fig. 2(c), the k-points on the plane where $b_2 \cdot \vec{k} = 0$ share nearly identical eigenvalues leading to flat bands along the lines from Z (0, 0, 0.5) to $\Gamma(0, 0, 0)$ and from B (-0.5, 0, 0) to D (-0.5, 0, 0.5). In the plane with $b_2 \cdot \vec{k} = 0.5$, on the border of the Brillouin zone, the bands from Y (0, 0.5, 0) to A (-0.5, 0.5, 0) and from E (-0.5, 0.5, 0.5) to C (0, 0.5, 0.5) are also flat, whereas significant band dispersion is found along all other k-paths. A schematic diagram of the Brillouin zone and high symmetry path for SANQII is provided in Fig. S3 in the SI.

In contrast to FANNUL, SANQII exhibits significant qualitative changes in the band structure at the same pressures where the discontinuous changes in the lattice parameters occur. The π -stacking along the b direction is preserved throughout the entire pressure range and even enhanced at the transition pressure as evident from discontinuous increase in the C···C contacts shown in Fig. S4(a) in the SI. Therefore, the bands along paths on the two planes with $b_2 \cdot \vec{k} = 0$ and $b_2 \cdot \vec{k} = 0.5$ remain flat. However, the VBM changes from k points on the plane with $b_2 \cdot \overline{k} =$ 0.5 to the plane with $b_2 \cdot \vec{k} = 0$, while the CBM switches from the plane with $b_2 \cdot \vec{k}$ = 0 to the plane with $b_2 \cdot \vec{k} = 0.5$. The dispersion also band exhibits discontinuous decrease from 7.5 to 8.0 GPa, as shown in Fig. 2(d). The valence band dispersion decreases by 0.204 eV and the conduction band dispersion decreases by 0.065 eV. As a result, the band gap increases discontinuously by 0.24 eV (see Fig. S4(b) in the SI). This may be related to the increased H···H interactions, which reduces the frontier orbital coupling (see Fig. S4(a) in the SI).

The significant qualitative change in the band structure can be explained by the trends in the H_{ab} values of both dimers, as shown in Fig. 2(e). The hole transfer H_{ab} value of dimer **a** decreases continuously until 7.5 GPa and

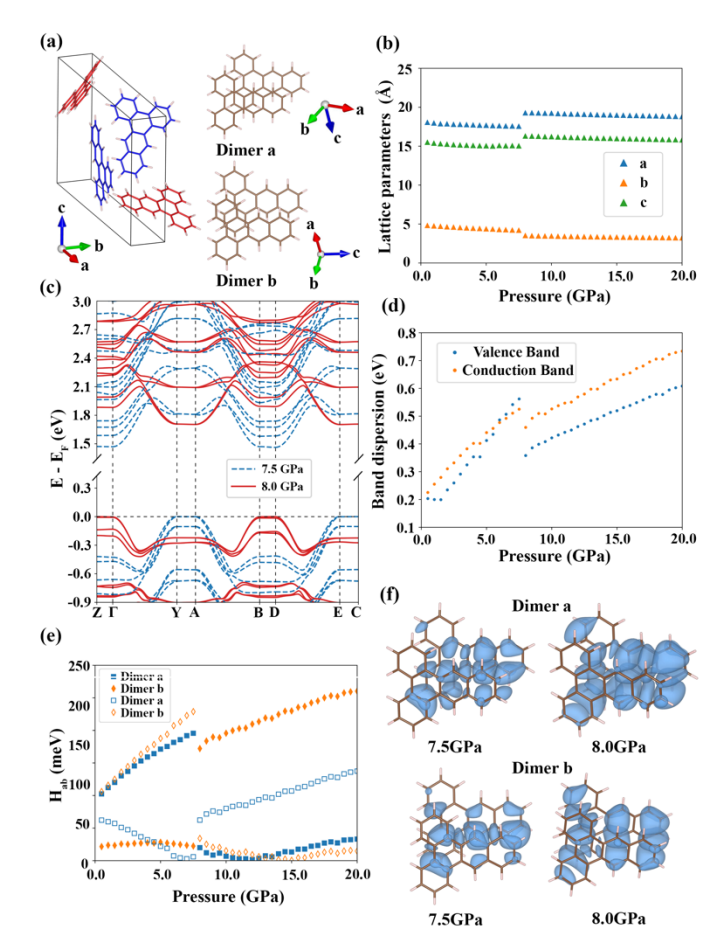


Fig. 2. (a) Equivalent molecules in the SANQII unit cell are shown in the same color. Both dimers **a** and **b** are stacked along the *b* direction. (b) Pressure dependence of the lattice parameters. (c) Band structures of SANQII at 7.5 GPa and 8.0 GPa with the VBM referenced to 0 eV. (d) The dispersion of HOMO derived valence band and LUMO derived conduction band as a function of pressure. (e) Pressure dependence of the electron/hole transfer H_{ab} of both dimers, the full marker represents the electron transfer H_{ab} and empty marker represents the hole transfer H_{ab}. (f) Overlap of HOMOs of two molecules in dimer **a** (left) and **b** (right) at 7.5 GPa and 8.0 GPa.

then increases by 56.4 meV at 8.0 GPa. Simultaneously, an abrupt decrease of 194.7 meV is observed at the same pressure in the hole transfer H_{ab} value of dimer **b**. The electron transfer H_{ab} of dimer **a** drops by 175.64 meV at the same discontinuity while the electron transfer H_{ab} of dimer **b** increases by 149.75 meV. The hole transfer H_{ab} dominates at pressures below the discontinuity, whereas the electron transfer H_{ab} dominates above the discontinuity. This indicates a switch of polarity, which is also evident from the change of band dispersion shown in Fig. 2(d). Specifically, the HOMO derived valence band dispersion is larger than the LUMO derived conduction band dispersion at 7.5 GPa but becomes smaller at 8.0 GPa, implying a switch from p- to n-type. Although the relative orientations of the dimers change only slightly from 7.5 to 8.0 GPa, large differences are observed in the HOMO overlap for both dimers, as shown in Fig. 2(f) (additional

views of the orbital overlap of both dimers are provided in Fig. S5 in the SI). This results in the discontinuous changes of the electronic properties. Here, the H_{ab} values not only capture the pressure at which the change in the band structure occurs, as do the structural descriptors, but also allow the identification of specific dimers whose electronic couplings contribute to the change.

3.1.3. 1,8-Dipyrenylnaphthalene (CENYAV)

CENYAV has a monoclinic crystal structure with the space group of P2₁ and two molecules per unit cell, as shown in Fig. 3(a). The CENYAV molecule can be regarded as a pyrene substituted naphthalene. The frontier orbitals are mainly localized on the pyrene moieties as shown in Fig. S6

in the SI. In Fig. 3(a), three unique CENYAV dimers are viewed perpendicular to the naphthalene cores at their initial configuration at 0 GPa. In dimer a, the pyrene moieties of both molecules are parallel to each other. The pyrene moieties in dimer **b** and dimer c are both perpendicular to each other with closest contacts (C···H type) occurring between the pyrene moieties in dimer **b** and closest contacts (C···H type) occurring between pyrene and naphthalene in dimer c. C.-. H interactions are also observed between the naphthalene core of one molecule and the pyrene moieties of the other in dimer c in this view. The pressure dependence of the lattice parameters a, b, and c for CENYAV is plotted in Fig. 3(b). The three lattice parameters decrease nearly continuously at pressures below 9.5 GPa and above 10.0 GPa. From 9.5 to 10.0 GPa, discontinuous decreases of 6.7% and 7.1% occur for the a and b parameters, while the c parameter increases discontinuously by 10.6%. These structural changes also manifest in the Hirshfeld surface intermolecular close contact fractions, shown in Fig. S7(a) in the SI.

Due to the forced sandwich herringbone-like packing of the pyrene moieties in the *ac* plane, and the fact that the frontier molecular orbitals are localized on these moieties, the band structure of CENYAV exhibits dispersed bands along all paths in the Brillouin zone at energies near the band gap, as shown in Fig. 3(c). As the pressure increases from 9.5 to 10.0 GPa, the dispersion of the HOMO derived bands

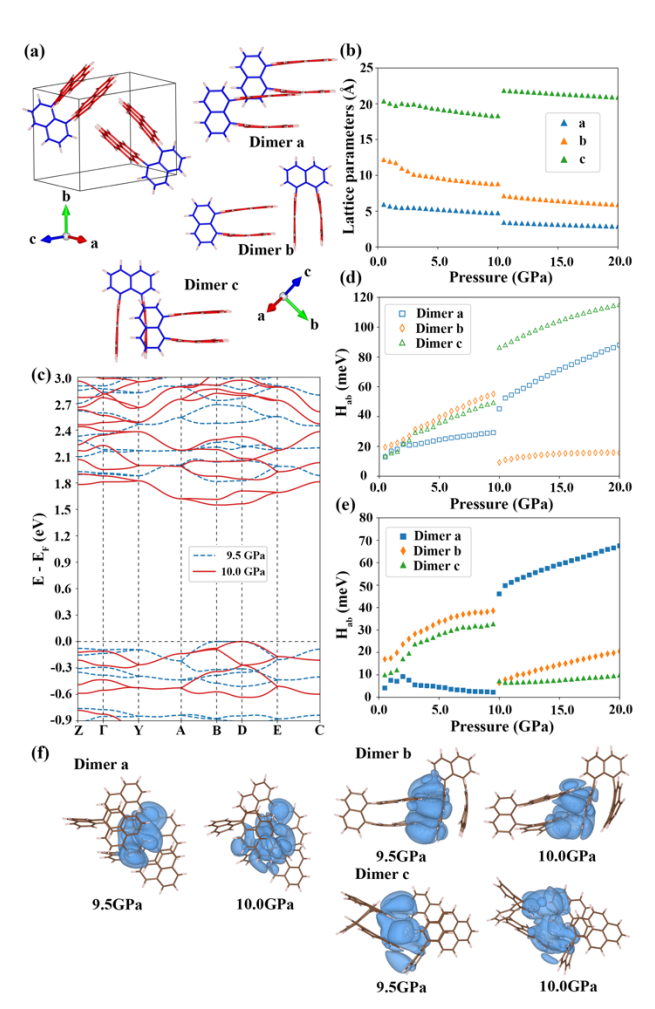


Fig. 3. (a) The CENYAV unit cell and three unique dimers. The pyrene moieties are colored in red and the naphthalene core is colored in blue. (b) Pressure dependence of the lattice parameters. (c) Band structures of CENYAV at 9.5 GPa and 10.0 GPa with the VBM referenced to 0 eV. (d) Pressure dependence of the hole transfer H_{ab} of the three dimers. (e) Pressure dependence of the electron transfer H_{ab} of the three dimers. (f) Overlap of the HOMOs of the molecules in dimer **a** (left), dimer **b** (top right) and dimer **c** (bottom right) at 9.5 and 10.0 GPa.

increases by 0.045 eV, and the dispersion of the LUMO derived bands increases by 0.088 eV, contributing to the narrowing of the band gap (see also Fig. S7 in the SI). Moreover, the VBM relocates from point B to D, whereas the CBM remains at point B, which changes the gap from direct to indirect.

The pressure dependence of electron and hole transfer H_{ab} values is plotted in Figs. 3(d) and 3(e) for the three dimers in Fig. 3(a). Discontinuities appear between 9.5 to 10 GPa. The hole transfer H_{ab} value of dimer **b** decreases by 46.1 meV, whereas the hole transfer H_{ab} values of dimer **a** and dimer **c** increase by 16.0 and 27.0 meV, respectively. The electron transfer H_{ab} , value of dimer **a** increases by 45.15 eV, from 9.5 to 10 GPa, whereas the electron transfer H_{ab} values of dimer **b** and dimer **c** decrease by 32.15 and 25.4 meV, respectively. The hole transfer H_{ab} of the three dimers dominates at all pressures, implying that CENYAV is a *p*-type semiconductor. This is also reflected in the pressure dependence of the band dispersion, shown in Fig. S7 in the SI. The change in the HOMO overlaps, shown in Fig. 3(f), is positively correlated with the change in H_{ab} .

CENYAV undergoes significant conformational changes with increased pressure (See Fig. S8 in SI and Refs ¹³ and ¹⁵). Therefore, to elucidate the influence of the molecular orbital energies on the electronic properties, single molecule calculations were performed for the structures at 0.5 and 20.0 GPa. The single molecule HOMO–LUMO gaps at 0.5 and 20.0 GPa are 2.306 and 2.145 eV, respectively. The HOMO–LUMO gap decreases by 0.16 eV from 0.5 to 20.0 GPa, whereas the bulk band gap decreases by 0.79 eV over the same pressure range. This indicates that the change in the band structure may be attributed primarily to the changes in the intermolecular coupling, and to a lesser extent to the changes in the molecular conformation.

3.2. Band structure changes not accompanied by significant discontinuities in the lattice parameters

3.2.1. 9-(4-Biphenyl)cyclopenta[a]phenalene (ABECAL)

The ABECAL crystal has a monoclinic structure with a P2₁/n space group and four molecules per unit cell, as shown in Fig. 4(a). ABECAL, like SANQII, exhibits significant $\pi^{...}\pi$ stacking for a HB PAH,⁵³ owing to cofacial intermolecular interactions, which are visible in the *bc* plane in Fig. 4(a). The pressure-dependence of the $\pi^{...}\pi$ interactions is reflected in the C···C% values obtained from Hirshfeld surface analysis, shown in Fig. S9 in the SI. Two dimers are displayed in the *ac* plane in Fig. 4(a). There is no distinct π -stacking between the molecules in dimer **a**, whereas dimer **b** shows co-facial π -stacking of the phenalene moieties of both molecules.

ABECAL exhibits more moderate lattice parameter changes than FANNUL, SANQII, and CENYAV under increasing pressure, as shown in Fig. 4(b). Between 5.5 and 6.0 GPa, the *b* and *c* lattice parameters increase by 0.7% and 1.2%, respectively, while the *a* lattice parameter decreases by 3.2%. Several minor discontinuities are also observed in the *c* lattice parameter. The comparatively small changes in the lattice parameters of ABECAL also manifest in relatively small pressure-dependent discontinuities in the C···C and C···H intermolecular close contact fractions, as shown in Fig. S9 in the SI.

The structural discontinuities between 5.5 GPa to 6.0 GPa correspond to a qualitative change in the band structure of ABECAL, where the VBM transfers from a k-point on the A-B path to the k-point E(-0.5, 0.5, 0.5), as shown in Fig. 4(c). Interestingly, two additional qualitative changes in the band structure are not accompanied by pressure-dependent discontinuities in the lattice parameters. First, between 6.5 GPa to 7.0 GPa, the VBM transfers back to the A-B segment. Then, between 8.5 GPa to 9.0 GPa, the VBM moves again to k-point B. The positions of the VBM at different pressures are labeled in Fig. 4(c) and additional band structures are provided in Fig. S10 in the SI.

The Hab values, in particular for dimer b, reveal the two additional discontinuities between 6.0 GPa and 9.0 GPa, as shown in Fig. 4(d). The C···H intermolecular close contacts also exhibit discontinuities at similar pressures, as shown in Fig. S9 in the SI. The magnitude of the hole transfer Hab is larger than the electron transfer Hab for both dimers below 6 GPa, at which point a polarity switching occurs and the electron transfer Hab becomes larger. Therefore, ABECAL transitions from a p-type to an n-type semiconductor. This is also evident from Fig. 4(e), as the LUMO-derived conduction band becomes more dispersed than the HOMO-derived valence band above 6 GPa.

Fig. 4(f) shows that the discontinuities in the Hab values of dimer **b** correspond to noticeable changes in the overlap of the HOMO orbitals, although the internal geometric change is relatively small. The overlap of the HOMO orbitals does not change significantly from 0.5 to 5.5 GPa, where the Hab changes almost continuously. Between 5.5 and 9.5 GPa, where discontinuities occur, the overlap decreases noticeably, as indicated by the red circles in Fig. 4(f). Above 9 GPa, where the Hab changes continuously again, the overlap of the HOMO orbitals remains almost unchanged. The case of ABECAL demonstrates that Hab is a predictive descriptor of pressure-induced

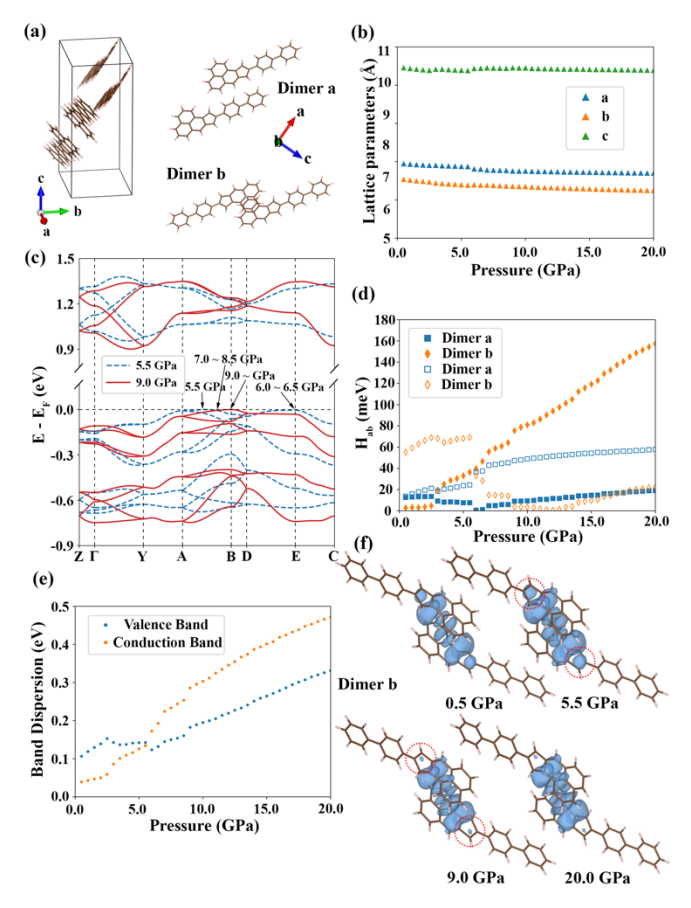


Fig. 4. (a) The ABECAL unit cell. Dimers **a** and **b** are viewed from the *b* direction (b) Pressure dependence of the lattice parameters. (c) Band structures of ABECAL at 5.5 GPa and 9.0 GPa with the VBM referenced to 0 eV. Arrows indicate the position of the VBM at different pressures. (d) Pressure dependence of the electron/hole transfer H_{ab} of dimers **a** and **b**, the full marker represents the electron transfer H_{ab} and empty marker represents the hole transfer H_{ab}. (e) The dispersion of HOMO derived valence band and LUMO derived conduction band as a function of pressure. (f) Overlap of HOMOs of two molecules in dimer **b** at different pressures.

changes in the band structure because it is sensitive to minor internal structural changes within the unit cell that do not necessarily correspond to discontinuities in the lattice parameters.

3.2.2. [5] Helicene (DBPHEN02)

[5]Helicene is comprised of five aromatic rings in a helical structure. 54 Fig. 5(a) depicts the monoclinic polymorph with a P2₁/c space group and four molecules per unit cell. Dimer **a** consists of two neighboring molecules stacked along the *a* direction. The pressure dependence of the three lattice parameters is shown in Fig. 5(b). The *c* lattice parameter decreases continuously by 9.5% as the pressure increases from 0.0 to 20.0 GPa. The *a* and *b* parameters exhibit some minor

discontinuities between 5.0 and 12.0 GPa, the largest of which is less than 2.0%. Thus, the lattice parameters of DBPHEN02 may be regarded as varying continuously, compared to the previous Likewise, the close contact cases. fractions of DBPHEN02 have nearly continuous pressure-dependent changes, for relatively minor except a discontinuous change in the C···C contacts between 6.5-7.0 GPa, as shown in Fig S11 in the SI.

Despite the nearly continuous pressure dependence of the structural the band structure descriptors, DBPHEN02 exhibits a qualitative change as the pressure increases from 6.5 to 7.0 GPa, as shown in Fig. 5(c). This is also apparent in the pressure dependence of the band gap, shown in Fig. 5(d)). Three pressure regimes are observed: Below 6.5 GPa the VBM is located at the Γ point. Between 6.5 and 7.0 GPa, the VBM transfers from the Γ point to the point (-0.26, 0.5, 0.5) on the E-C segment. Above 7.0 GPa, as the pressure increases, the VBM gradually moves toward the point (-0.42, 0.5, 0.5) on the E-C segment. The VBM position in the two regimes is indicated in Fig. 5(c) and additional band structures are provided in Fig. S12 in the SI.

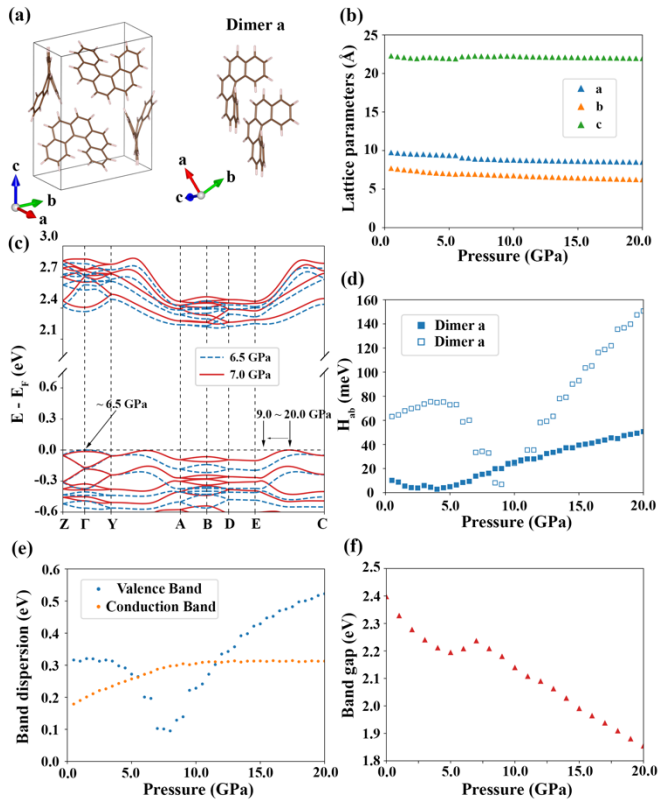


Fig. 5. (a) The DBPHEN02 unit cell. Dimer $\bf a$ is stacked along the a direction. (b) Pressure dependence of the lattice parameters. (c) Band structures of DBPHEN02 at 6.5 GPa and 7.0 GPa with the VBM referenced to 0 eV. (d) PBE derived band gap as a function of pressure. (e) Pressure dependence of the electron/hole transfer H_{ab} of dimer $\bf a$, the full marker represents the electron transfer H_{ab} and empty marker represents the hole transfer H_{ab} . (f) The dispersion of HOMO derived valence band and LUMO derived conduction band as a function of pressure.

The three pressure regimes, which cannot be discerned from the pressure dependence of the structural descriptors, are clearly visible in the pressure dependence of the hole transfer H_{ab} value of dimer $\bf a$ in Fig. 5(e). The hole transfer H_{ab} increases slowly up to 6.5 GPa, then decreases from 7.0 GPa to 9.0 GPa, and finally increases from 9.5 GPa to 20 GPa in a similar manner to the HOMO-derived band dispersion, shown in Fig. 5(f). Several discontinuities occur in H_{ab} when the VBM transfers from point to point within each segment. Each minor discontinuity above 7.0 GPa corresponds to a slight change of the position of the VBM on the E-C segment. The coordinates of the position of the VBM under different pressures are provided in Table S1 in the SI. The electron transfer H_{ab} shows a continuous trend as the pressure increases. Throughout most of the pressure range, DBPHEN02 exhibits p-type polarity, with the hole transfer H_{ab} having higher values than electron transfer H_{ab} . However, polarity switching occurs between 5.5 and 11.5 GPa, where the electron transfer H_{ab} dominates. This is consistent with the changes in the band dispersion, shown in Fig. 5(f). Owing to the gradual quantitative change in H_{ab} , the difference in the HOMO overlap between the molecules of dimer $\bf a$ is not as obvious as in other cases studied

here. An increase in the HOMO overlap is still noticeable between 5.5 GPa and 8.5 GPa, as shown in Fig. S11(a). This demonstrates yet again that H_{ab} can capture small structural changes that lead to qualitative changes in the electronic properties of molecular crystals.

3.2.3. 7,14-Diphenyldibenzo[de,mn]naphthacene (KAGFOP)

KAGFOP has a monoclinic crystal structure with the space group of P2₁/n and four molecules per cell, as shown in Fig. 6(a). The molecule is comprised of a twisted zethrene backbone, colored in dark blue, and two phenyl side groups, colored in light blue. The frontier orbitals are mainly localized on the zethrene backbone, as shown in Fig. S13 in the SI. Two dimers, labeled **a** and **b**, are shown in their 0 GPa configuration. Dimer **a** comprises a pair of neighboring molecules stacked in the *c* direction. Dimer **b** comprises a pair of neighboring molecules along the *a* direction. Fig. 6(b) shows that the lattice parameters of KAGFOP decreases nearly continuously as a function of pressure. The *b* parameter decreases the most over the entire 20 GPa range (by 17.5%), whereas

the *a* and *c* lattice parameters decrease by 8.7% and 10.5%, respectively. Relatively minor discontinuities are visible in all parameters between 13.5 GPa to14.0 GPa. There are also relatively small discontinuities in the C···H and H···H intermolecular close contact fractions from 13.5 GPa to 14.0 GPa, as shown in Fig. S14(a) in the SI.

The band structure of KAGFOP at 13.5 GPa and 14 GPa is shown in Fig. 6(c). Additional representative band structures are provided in Fig. S5 in the SI. Along the segment from D (-0.5, 0, 0.5) to E (-0.5, 0.5, 0.5) the bands are nearly flat throughout the 0-20 GPa pressure range. This direction is along b_2 in the Brillouin zone, which corresponds to the b direction in real space. Along this direction, the presence of two phenyl side groups impedes the overlap of the frontier orbitals, which are localized on the zethrene backbones, leading to weak intermolecular electronic coupling and flat bands. In contrast, the bands are more dispersed along other directions. To highlight the discontinuous nature of the band structure between 13.5-14.0 GPa, the energy difference between the local VBM at points Γ (0, 0, 0) and N (-0.5, 0, 0.45) is plotted in Fig. 6(d). The positive energy difference from 0 to 4.0 GPa, indicates that the VBM is located

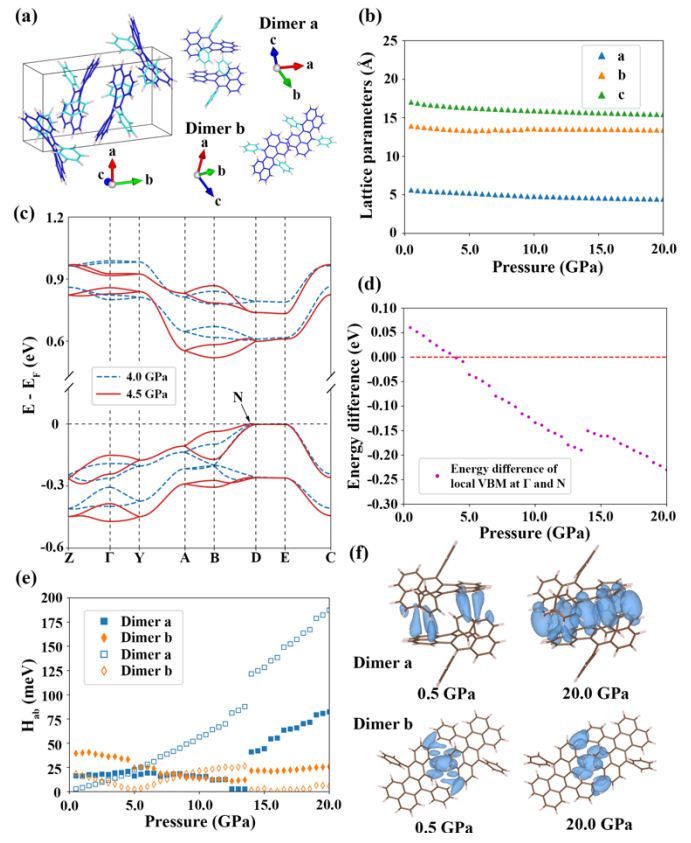


Fig. 6. (a) The KAGFOP unit cell. The zethrene backbones are colored in dark blue and the phenyl side groups in light blue. Both dimers $\bf a$ and $\bf b$ are stacked in the ac plane. (b) Pressure dependence of the lattice parameters. (c) Band structures of KAGFOP at 13.5 GPa and 14.0 GPa with the VBM referenced to 0 eV. (d) Energy difference of the local VBM at points Γ and N. (e) Dependence of the electron/hole transfer H_{ab} of both dimers on pressure, the full marker represents the electron transfer H_{ab} and empty marker represents the hole transfer H_{ab} . (f) Overlap of the HOMOs of the molecules in dimer $\bf a$ (top) and $\bf b$ (bottom) at 13.5 GPa and 14.0 GPa.

at point Γ . Above 4.0 GPa, the energy difference becomes negative as the VBM transfers from Γ to N. Minor discontinuities are found at 5 GPa, 7 GPa, and 12.5 GPa. The most significant discontinuity occurs between 13.5-14.0 GPa, resulting in an increase of 0.07 eV in the HOMO derived band dispersion and 0.07 eV in the LUMO derived band dispersion, accompanied by a reduction of 0.10 eV in the band gap, as shown in Fig. S14(b) in the SI.

Fig. 6(e) shows the electron and hole transfer Hab values of dimers a and b as a function of pressure. The considerable change in the hole transfer Hab of dimer a from near zero initially to almost 200 meV at 20 GPa implies major changes in the electronic properties across the pressure range, although the changes are not always discontinuous. The minimum in the hole transfer Hab of dimer **b** at 5.0 GPa is consistent with the discontinuity observed in the band structure. The minor discontinuity in the hole transfer H_{ab} of dimer a around 12.5 GPa is consistent with the minor discontinuity in the band structure. The minor discontinuity in the band structure around 7 GPa is captured by the electron transfer H_{ab} of both dimers. All dimers exhibit significant discontinuities between 13.5 GPa and 14.0 GPa, in agreement with the major discontinuity in the band structure. The electron transfer H_{ab} shows good agreement with all the discontinuities observed in the hole transfer H_{ab}, although it has relatively low values for both dimers. Fig. 6(f) shows the HOMO overlap for both dimers at 0.5 GPa and 20 GPa. Both dimers exhibit a noticeable change. The overlap in dimer a is much larger than in dimer b due to the co-facial interaction between the zethrene backbones. For KAGFOP, Hab is again more revealing than the lattice parameters of relatively small internal structural changes that lead to significant changes in the intermolecular coupling and, as a result, in the electronic properties.

4. Conclusion

In summary, for six PAH crystals with a herringbone packing motif, FANNUL, SANQII, CENYAV, ABECAL, DBPHEN02, and KAGFOP, we have investigated the correlations between the pressure dependence of the lattice parameters, band structures, and intermolecular electronic couplings, represented by the transfer matrix elements, H_{ab}. In the pressure range of up to 20 GPa the band structures of all six PAHs exhibit discontinuous changes. For FANNUL, SANQII, and CENYAV the discontinuous changes in the band structure correspond to significant discontinuous changes in the structural descriptors, whereas ABECAL, DBPHEN02, and KAGFOP exhibit discontinuous changes in the electronic properties that are not accompanied by significant discontinuities in the pressure dependence of the structural descriptors. For all six systems, discontinuous changes in the band structure are correlated with discontinuities in the pressure dependence of the H_{ab} values of certain dimers.

Based on this, we conclude that H_{ab} is a reliable descriptor to gain insight into the pressure dependence of electronic properties of crystalline organic semiconductors. H_{ab} is sensitive to internal structural changes that do not necessarily correspond to significant changes in the lattice parameters or intermolecular close contact fractions, and yet lead to significant changes in the intermolecular electronic coupling, which result in changes in the electronic properties. H_{ab} values can resolve the effect of intermolecular interactions from that of intramolecular conformational changes and help identify the specific dimers that have the largest contribution towards changes in the electronic properties. The computational cost of calculating H_{ab} using fragment orbital DFT is lower than that of band structure calculations and the results are easier to analyze via an automated process. Therefore, we find H_{ab} to be a useful tool for high-throughout studies of molecular crystals.

Acknowledgements

Work at CMU was funded by the National Science Foundation (NSF) Division of Materials Research through Grant No. DMR-1554428. Work at CPP was funded by NSF Division of Materials Research through Grant No. DMR-1637026. This research used resources of the National Energy Research Scientific Computing Center (NERSC), a DOE Office of Science User Facility supported by the Office of Science of the U.S. Department of Energy under Contract No. DE-AC02-05CH11231.

References

- 1. Bergantin, S., Moret, M., Buth, G. & Fabbiani, F. P. A. Pressure-induced conformational change in organic semiconductors: Triggering a reversible phase transition in rubrene. *J. Phys. Chem. C* **118**, 13476–13483 (2014).
- 2. Schwarze, M. et al. organic semiconductors. **352**, 1446–1450 (2016).
- 3. Anthony, J. E. The larger acenes: Versatile organic semiconductors. *Angew. Chemie Int. Ed.* **47**, 452–483 (2008).
- 4. Kroon, R., Lenes, M., Hummelen, J. C., Blom, P. W. M. & De Boer, B. Small bandgap polymers for organic solar cells (polymer material development in the last 5 years). Polymer Reviews 48, 531–582 (2008).
- 5. Henson, Z. B., Müllen, K. & Bazan, G. C. Design strategies for organic semiconductors beyond the molecular formula. *Nat. Chem.* **4**, 699–704 (2012).
- 6. Mishra, A. & Bäuerle, P. Small molecule organic semiconductors on the move: Promises for future solar energy technology. *Angew. Chemie Int. Ed.* **51,** 2020–2067 (2012).
- 7. Zhou, H., Yang, L. & You, W. Rational design of high performance conjugated polymers for organic solar cells. *Macromolecules* **45**, 607–632 (2012).
- 8. Beaujuge, P. M. & Fréchet, J. M. J. Molecular design and ordering effects in π -functional materials for transistor and solar cell applications. *J. Am. Chem. Soc.* **133**, 20009–20029 (2011).
- 9. Pfattner, R. *et al.* High-performance single crystal organic field-effect transistors based on two dithiophene-tetrathiafulvalene (DT-TTF) polymorphs. *Adv. Mater.* **22**, 4198–4203 (2010).
- 10. Li, Y. *et al.* Quick Fabrication of Large-area Organic Semiconductor Single Crystal Arrays with a Rapid Annealing Self-Solution-Shearing Method. *Sci. Rep.* **5**, 1–9 (2015).
- 11. Curtis, F., Wang, X. & Marom, N. Effect of packing motifs on the energy ranking and electronic properties of putative crystal structures of tricyano-1,4-dithiino[c]-isothiazole. *Acta Crystallogr. Sect. B Struct. Sci. Cryst. Eng. Mater.* 72, 562–570 (2016).
- 12. Anthony, J. E. Functionalized acenes and heteroacenes for organic electronics. *Chem. Rev.* **106,** 5028–5048 (2006).
- 13. Hammouri, M. *et al.* High-Throughput Pressure Dependent DFT Investigation of Herringbone Polycyclic Aromatic Hydrocarbons (HB-PAHs): Part 2. Pressure Dependent Electronic Properties. *J. Phys. Chem. C* **42**, 23828–23844 (2018).
- 14. Brillante, A. *et al.* High-pressure dissociation of crystalline para-diiodobenzene: Optical experiments and car-parrinello calculations. *J. Am. Chem. Soc.* **127,** 3038–3043 (2005).
- 15. Hammouri, M. *et al.* High-Throughput Pressure Dependent DFT Investigation of Herringbone Polycyclic Aromatic Hydrocarbons (HB-PAHs): Part 1. Pressure Dependent Structure Trends. *J. Phys. Chem. C* **42**, 23815–23827 (2018).
- 16. Schatschneider, B., Monaco, S., Tkatchenko, A. & Liang, J. J. Understanding the structure

- and electronic properties of molecular crystals under pressure: Application of dispersion corrected DFT to oligoacenes. *J. Phys. Chem. A* **117**, 8323–8331 (2013).
- 17. Nguyen, T. P. & Shim, J. H. Hydrostatic pressure effect on charge transport properties of phenacene organic semiconductors. *Phys. Chem. Chem. Phys.* **18**, 13888–13896 (2016).
- 18. Rang, Z. *et al.* Hydrostatic-pressure dependence of the photoconductivity of single-crystal pentacene and tetracene. *Appl. Phys. Lett.* **79**, 2731–2733 (2001).
- 19. Cui, X., Xiao, C., Zhang, L., Li, Y. & Wang, Z. Polycyclic aromatic hydrocarbons with orthogonal tetraimides as n-type semiconductors. *Chem. Commun.* **52**, 13209–13212 (2016).
- 20. Delaunay, W. *et al.* Synthesis and electronic properties of polycyclic aromatic hydrocarbons doped with phosphorus and sulfur. *Dalt. Trans.* **45,** 1896–1903 (2016).
- 21. Wu, J., Pisula, W. & Müllen, K. Graphenes as potential material for electronics. *Chem. Rev.* **107,** 718–747 (2007).
- 22. Li, Y., Clevenger, R. G., Jin, L., Kilway, K. V. & Peng, Z. Spin-Coated Thin Films of Polycyclic Aromatic Hydrocarbons Exhibiting High SCLC Hole Mobilities. *J. Phys. Chem. C* 120, 841–852 (2016).
- 23. Moreno, I. & Sun, C.-C. Modeling the radiation pattern of LEDs. *Opt. Express* **16,** 1808 (2008).
- 24. Fanetti, S. *et al.* High-Pressure Optical Properties and Chemical Stability of Picene. *J. Phys. Chem. C* **117**, 5343–5351 (2013).
- 25. Lynch, R. W. & Drickamer, H. G. Effect of high pressure on the lattice parameters of diamond, graphite, and hexagonal boron nitride. *J. Chem. Phys.* **44**, 181–184 (1966).
- 26. Dalven, R. Empirical relation between energy gap and lattice constant in cubic semiconductors. *Phys. Rev. B* **8**, 6033–6034 (1973).
- 27. Schober, C. *et al.* Critical analysis of fragment-orbital DFT schemes for the calculation of electronic coupling values Critical analysis of fragment-orbital DFT schemes for the calculation of electronic coupling values. *J. Chem. Phys.* **144**, 054103, (2017).
- 28. Kubas, A. *et al.* Electronic couplings for molecular charge transfer: Benchmarking CDFT, FODFT and FODFTB against high-level ab initio calculations. II. *Phys. Chem. Chem. Phys.* **17**, 14342–14354 (2015).
- 29. Sa, R. S., Atahan, S. & Schrier, J. Theoretical Characterization of the Air-Stable, High-Mobility Dinaphtho [2, 3-b:2'3'-f] thieno [3, 2-b]-thiophene Organic Semiconductor. *J. Phys. Chem. C* 114, 2334–2340 (2010).
- 30. McGarry, K. A. *et al.* Rubrene-based single-crystal organic semiconductors: Synthesis, electronic structure, and charge-transport properties. *Chem. Mater.* **25**, 2254–2263 (2013).
- 31. Schober, C., Reuter, K. & Oberhofer, H. Virtual Screening for High Carrier Mobility in Organic Semiconductors. *J. Phys. Chem. Lett.* **7**, 3973–3977 (2016).
- 32. Zhu, T., Van Voorhis, T. & de Silva, P. Charge Transfer in Molecular Materials. *Handbook of Materials Modeling. Springer, Cham* 1-31 (2018).
- 33. Oberhofer, H., Reuter, K. & Blumberger, J. Charge Transport in Molecular Materials: An Assessment of Computational Methods. *Chem. Rev.* **117**, 10319–10357 (2017).
- 34. Shea, K. M., Lee, K. L. & Danheiser, R. L. Synthesis and Properties of 9-Alkyl- and 9-Arylcyclopenta[a]phenalenes. *Org. Lett.* **2**, 2353–2356 (2000).
- 35. Kuroda, R. Crystal and molecular structure of [5]helicene: crystal packing modes. *J. Chem. Soc. Perkin Trans.* **2**, 789 (1982).
- 36. Wahl, P., Krieger, C., Schweitzer, D. & Staab, H. A. 1,8-Dipyrenylnaphthalenes: Syntheses, Molecular Structure, and Spectroscopic Properties. *Chem. Ber.* **117**, 260–276 (1984).

- 37. Fernandes, P., Florence, A., Shankland, K. & David, W. I. F. Powder diffraction study of 1,2:3,4-dibenzanthracene. *Acta Crystallogr. Sect. E Struct. Reports Online* **61**, 1483–1485 (2005).
- 38. Wu, T. C. *et al.* Synthesis, structure, and photophysical properties of dibenzo-[de, mn]naphthacenes. *Angew. Chemie Int. Ed.* **49**, 7059–7062 (2010).
- 39. Chiang, C. C. & Paul, I. C. Crystal and molecular structure of [14]annulene. *J. Am. Chem. Soc.* **94,** 4741–4743 (1972).
- 40. Clark, S. J. et al. First principles methods using CASTEP. Zeitschrift fur Krist. 220, 567–570 (2005).
- 41. Perdew, J. P., Burke, K. & Ernzerhof, M. Generalized gradient approximation made simple. *Phys. Rev. Lett.* **77**, 3865–3868 (1996).
- 42. Tkatchenko, A. & Scheffler, M. Accurate molecular van der Waals interactions from ground-state electron density and free-atom reference data. *Phys. Rev. Lett.* **102**, 6–9 (2009).
- 43. Zhang, I. Y., Ren, X., Rinke, P., Blum, V. & Scheffler, M. Numeric atom-centered-orbital basis sets with valence-correlation consistency from H to Ar. *New J. Phys.* **15**, 123033 (2013).
- 44. Blum, V. et al. Ab initio molecular simulations with numeric atom-centered orbitals. *Comput. Phys. Commun.* **180**, 2175–2196 (2009).
- 45. Senthilkumar, K., Grozema, F. C., Bickelhaupt, F. M. & Siebbeles, L. D. A. Charge transport in columnar stacked triphenylenes: Effects of conformational fluctuations on charge transfer integrals and site energies. *J. Chem. Phys.* **119**, 9809–9817 (2003).
- 46. Oberhofer, H. & Blumberger, J. Revisiting electronic couplings and incoherent hopping models for electron transport in crystalline C60at ambient temperatures. *Phys. Chem. Chem. Phys.* **14**, 13846–13852 (2012).
- 47. Becke, A. D. Density-functional exchange-energy approximation with correct asymptotic behavior. *Phys. Rev. A* **38**, 3098–3100 (1988).
- 48. Lee, C., Yang, W. & Parr, R. G. Development of the Colle-Salvetti correlation-energy formula into a functional of the electron density. *Phys. Rev. B* **37**, 785–789 (1988).
- 49. McKinnon, J. J., Jayatilaka, D. & Spackman, M. A. Towards quantitative analysis of intermolecular interactions with Hirshfeld surfaces. *Chem. Commun.* **0**, 3814–3816 (2007). doi:10.1039/b704980c
- 50. Spackman, M. A. & Jayatilaka, D. Hirshfeld surface analysis. *CrystEngComm* 11, 19–32 (2009).
- 51. M. J. Turner, J. J. McKinnon, S. K. Wolff, D. J. Grimwood, P. R. Spackman, D. J. and M. A. S. CrystalExplorer17. *University of Western Australia* (2017).
- 52. Gellini, C. & Salvi, P. R. Structures of annulenes and model annulene systems in the ground and lowest excited states. *Symmetry (Basel)*. **2**, 1846–1924 (2010).
- 53. Schatschneider, B., Phelps, J. & Jezowski, S. A new parameter for classification of polycyclic aromatic hydrocarbon crystalline motifs: A Hirshfeld surface investigation. *CrystEngComm* **13**, 7216–7223 (2011).
- 54. Chen, C. F. & Shen, Y. Helicene chemistry: From synthesis to applications. *Helicene Chem. From Synth. to Appl.* 1–272 (2016). doi:10.1007/978-3-662-53168-6